MOLECULAR PHARMACOLOGY, 14, 514-529

Kinetic Analysis of End Plate Currents Altered by Atropine and Scopolamine

M. ADLER, E. X. ALBUQUERQUE, AND F. J. LEBEDA[1]

Department of Pharmacology and Experimental Therapeutics, University of Maryland School of Medicine, Baltimore, Maryland 21201

(Received July 29, 1977)
(Accepted January 17, 1978)

SUMMARY

ADLER, M., ALBUQUERQUE, E. X. & LEBEDA, F. J. (1978) Kinetic analysis of end plate currents altered by atropine and scopolamine. *Mol. Pharmacol.*, 14, 514-529.

The decay phase of end plate currents in voltage-clamped frog sartorius muscle follows a single exponential function whose rate varies with membrane potential. Atropine increased the end plate current decay rate and reduced its voltage sensitivity, but did not alter its exponential nature. Scopolamine transformed the end plate current decay into a biphasic waveform consisting of a rapid initial current, followed by a slow terminal current. Two kinetic models were examined for their ability to simulate these drug-induced alterations of the end plate current. The models were formulated on the assumption that the drug molecules bind to the activated transmitter-receptor complex and induce sequential conversion of the end plate channel from a transient state of high conductance to a prolonged state of low or zero conductance. Drug binding was irreversible according to model I, and the complex of drug with the end plate channel was partially conducting. In model II the binding step was made reversible, and the resulting drug-channel complex was considered to be nonconducting. The predictions from these kinetic models were compared with data from voltage-clamped end plates. The theoretical end plate currents from model II agreed closely with experimental values, while those from model I were in conflict with the data.

INTRODUCTION

Considerable knowledge has been gained about the kinetic properties of the channel coupled to the acetylcholine receptor from studies on drugs and toxins that modify the time course of the end plate potential and associated end plate current. Alterations in the time course of the junctional response were noted for the local anesthetics (1-6), the belladonna alkaloids (7-14), and the histrionicotoxins (15-17).

This work was supported by Grant NS-12063 from the National Institutes of Health and a grant from the Muscular Dystrophy Association of America.

[1] Present address, Marine Biomedical Institute, Galveston, Texas 77550.

Although the above compounds possess a variety of chemical structures, only two basic alterations have been observed on the EPC[2] kinetics: (a) atropine (9, 13), histrionicotoxin (16), and the lidocaine derivative QX-314 (4, 18, 19) shorten the EPC rise time and increase its decay rate without affecting its single exponential nature, and (b) procaine (6, 20, 21), the lidocaine derivative QX-222 (4, 18), and scopolamine (11, 13) shorten the EPC rise time but convert the decay to a multiexponential function consisting of at least two distinct components, one more rapid and another slower

[2] The abbreviations used are: EPC, end plate current; ACh, acetylcholine.

0026-895X/78/0143-0514$02.00/0

than the decay of control EPCs.

Until recently, the best kinetic model to account for EPCs thus altered was a sequential reaction scheme developed by Steinbach (5) for the lidocaine derivatives, shown in modified form below. Model I differs from Steinbach's original formulation by the inclusion of the ACh_nR complex and by the presence of voltage-sensitive steps. In the model system, rapid reaction of n acetylcholine molecules with receptors (R) results in the production of an inactive intermediate complex (ACh_nR), which is followed by a slower voltage-sensitive conformational change leading to the formation of the conducting species (ACh_nR^*). The decay phase of the normal EPC is assumed to reflect the conformational relaxation of ACh_nR^*, which is governed by the rate-limiting constant k_{-2} (22-24). According to model I, when drug (D) is present, the EPC decays by an alternative route, forming ACh_nR^*D. Depending on D, ACh_nR^*D may be inactive, resulting in EPCs with rapid single exponential decays, or partially active, producing biphasic decays.

This model was found to be incompatible with some of our data, especially its predictions of the effect of drug concentration on the terminal component of biphasic EPC decays (13, 25). Therefore it was considered worthwhile to modify the above reaction scheme to attempt to reconcile experiment and theory. In this paper an alternative scheme is presented that preserves the essential features of model I but introduces two important modifications. First, ACh_nR^*D is assumed to be inactive regardless of the drug used. Second, the dissociation of ACh_nR^*D is assumed to occur by removal of D and restoration of ACh_nR^*, rather than by dissociation to nACh, R, and D. In model II, the appearance of single or double exponential decay depends solely on k_{-3}. When k_{-3} is near zero, i.e., when drug dissociation is negligible, the EPCs will decay as single exponential functions of time; as k_{-3} becomes appreciable, the more rapid dissociation of drug will produce a slower decrease in the concentration of ACh_nR^* and lead to the appearance of a terminal decay component.

To determine whether model II can account for EPCs altered by atropine and scopolamine, the reaction scheme was expressed as a set of coupled first-order differential equations, which were solved with a digital computer. Adequacy of the model was judged by its ability to generate EPCs with single and double exponential decay and to simulate the effects of drug concentration and membrane potential.

METHODS

Electrophysiology

The experimental data were obtained at room temperature (20-23°) from glycerol-treated (26) sciatic nerve-sartorius muscle preparations of the frog *Rana pipiens*. The voltage clamp technique for the end plate region was similar to that developed by Takeuchi and Takeuchi (27) and has been described in detail in previous publications (13, 28). The time constant of the clamping circuit (10-90%) with 3-8 Mohm microelectrodes was less than 25 μsec. The normal Ringer's solution had the following composition: NaCl, 115.0 mM; KCl, 2.0 mM; $CaCl_2$, 1.8 mM; Na_2HPO_4, 1.3 mM; and NaH_2PO_4, 0.7 mM.

$$\text{Release} \longrightarrow n\,\text{ACh} + R \underset{k_{-1}}{\overset{k_1}{\rightleftharpoons}} \text{ACh}_nR \underset{k_{-2}}{\overset{k_2}{\rightleftharpoons}} \text{ACh}_nR^* \xrightarrow{D,\ k_3} \text{ACh}_nR^*D \xrightarrow{k_4} n\,\text{ACh} + R + D \qquad \text{(I)}$$

$$\downarrow k_h$$

(diffusion and hydrolysis)

$$\text{Release} \longrightarrow n\,\text{ACh} + R \underset{k_{-1}}{\overset{k_1}{\rightleftharpoons}} \text{ACh}_nR \underset{k_{-2}}{\overset{k_2}{\rightleftharpoons}} \text{ACh}_nR^* \underset{D,\ k_{-3}}{\overset{D,\ k_3}{\rightleftharpoons}} \text{ACh}_nR^*D \qquad \text{(II)}$$

$$\downarrow k_h$$

(diffusion and hydrolysis)

Atropine sulfate and scopolamine hydrobromide (Sigma Chemical Company) were prepared from refrigerated stock solutions at concentrations of 60 mM. Unless stated otherwise, all values are expressed as means ± standard errors. Biphasic decays were treated as the sum of two exponentials as described previously (13, 29).

Theoretical Considerations

Normal EPC. The reaction scheme of Magleby and Stevens (24) was used as the starting point for the analysis of the normal EPC. Both sequential models can be reduced to this reaction by removal of the parameter D. Because no independent measurements are available for the time course of ACh, R, ACh_nR, and ACh_nR^*, it is necessary to make some simplifying assumptions to evaluate the kinetic model. For this purpose, the relevant assumptions of Magleby and Stevens (24), Albuquerque *et al.* (30), and Dionne and Stevens (31) were adopted. (a) Conductance is directly proportional to the concentration of ACh_nR^*. (b) Two acetylcholine molecules (n) interact with one receptor, in a noncooperative fashion. (c) The cleft volume containing receptors is thoroughly mixed, so that partial differential equations are avoided. (d) Buffering of cleft acetylcholine concentration by binding to receptors and other molecules is negligible. (e) Hydrolysis is taken to be proportional to the acetylcholine concentration.

In addition, transmitter release was assumed to occur for 300 μsec and to cease abruptly thereafter. In the model system the rate of transmitter release (f) was set equal to the ratio of the total acetylcholine concentration and the release time (t_r), or

$$f = \frac{[ACh]_{tot}}{t_r} \qquad \text{for } t \leqq t_r$$

and

$$f = 0 \qquad \text{for } t > t_r$$

Use of this release function led to more realistic simulations of the EPC rising phase than the conventional assumption of "instantaneous" release (Fig. 1B). Based on assumed dimensions of the frog neuromuscular junction, the synaptic cleft volume was calculated to be 10^{-11} liter. The receptor population (R_{tot}) was taken as 3×10^7 molecules/end plate according to the radioautographic evidence of Barnard *et al.* (32, 33). ACh_{tot} was initially set at 4×10^6 molecules (200 quanta with 2×10^4 molecules/quantum) (34). This was raised to 4.11×10^6 molecules during the course of simulating control EPC waveforms, to obtain better agreement with experimental amplitudes. These dimensions were subsequently changed to concentration units.

The following series of equations describing model III was used to calculate the amount of conducting species. All the molecular terms except $[R]_{tot}$ were considered to be functions of time and were expressed as molar concentrations.

$$\frac{d[ACh]}{dt} = f + k_{-1}[ACh_nR] - (k_h[ACh] + k_1[ACh]^n[R]) \quad (1)$$

$$\frac{d[ACh_nR]}{dt} = k_1[ACh]^n[R] + k_{-2}[ACh_nR^*] - (k_2 + k_{-1})[ACh_nR] \quad (2)$$

$$\frac{d[ACh_nR^*]}{dt} = k_2[ACh_nR] - k_{-2}[ACh_nR^*] \quad (3)$$

$$[R]_{tot} = [R] + [ACh_nR] + [ACh_nR^*] \quad (4)$$

$$I = N[\gamma_{Na}(V - V_{Na}) + \gamma_K(V - V_K)] \quad (5)$$

where I is the end plate current, V is the holding potential, N is the number of ACh_nR^* molecules, γ_{Na} and γ_K are single-channel conductances for sodium and potassium, respectively ($\gamma_{Na} + \gamma_K = \gamma$), and V_{Na} and V_K are the respective equilibrium potentials for sodium and potassium (see Table 1). Additional equations were incor-

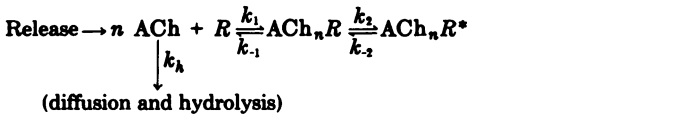

(III)

porated to describe the drug-acetylcholine-receptor complex in models I and II. Both schemes required the expression

$$\frac{d[\mathrm{ACh}_n R^* D]}{dt} = k_3\, D[\mathrm{ACh}_n R^*] - k_j\,[\mathrm{ACh}_n R^* D] \quad (6)$$

where k_j denotes k_4 in model I and k_{-3} in model II. In model I, Eq. 1 was modified to include the dissociation of this complex into the original reactants:

$$\frac{d[\mathrm{ACh}]}{dt} = f + k_{-1}[\mathrm{ACh}_n R] - (k_h[\mathrm{ACh}] + k_1[\mathrm{ACh}]^n[R]) + k_4[\mathrm{ACh}_n R^* D] \quad (1a)$$

In both models the amount of free drug changed with time according to

$$[D] = [D]_{t=0} - [\mathrm{ACh}_n R^* D] \quad (7)$$

Computational Techniques

Programming was performed on a PDP 11/40 digital computer (Digital Equipment Corporation, Maynard, Mass.) with 16,000 words of core memory running under a real-time, single-job-system monitor (RT-11SJ). The higher-level language used was an extended version of BASIC that made available data buffer areas and had graphics capabilities. The system monitor, BASIC, and all the BASIC model programs were stored on an RK05 cartridge disk.

For graphical displays of numerical solutions, digital-to-analogue conversions were made by an LPS-11 unit. The X and Y voltages from this unit were sent to a Tektronix type 564 storage oscilloscope with two 3A3 dual-differential preamplifiers. With this configuration, each incremental solution of the coupled differential equations could be displayed and stored without continuously refreshing the screen. When desired, the individual EPC waveforms were stored as a data file on the disc for later display or analysis.

The fundamental set of coupled first-order differential equations for the three models was written into a separate main program. These linear and nonlinear equations were initially solved by a Runge-Kutta numerical algorithm (35). Later it

TABLE 1

Summary of rate constants and parameters of kinetic models

The rate constants were selected to produce model EPCs resembling experimental data visually. Further details are provided under METHODS.

Parameters	Rate constants				
	Voltage-independent	Voltage-dependent			
		Model 1		Model II	
		Atropine or scopolamine		Atropine	Scopolamine
$[R]_{t=0} = 5.0 \times 10^{-6}$ M	$k_1 = 5.9 \times 10^6$ M^{-2} msec^{-1}	$k_2(0)$, msec^{-1}	0.9	0.9	0.9
$[\mathrm{ACh}]_{t=0} = 6.8 \times 10^{-7}$ M	$k_{-1} = 3$ msec^{-1}	A_2, mV^{-1}	2.5×10^{-3}	2.5×10^{-3}	2.5×10^{-3}
$t_r = 300$ μsec	$k_h = 15$ msec^{-1}	$k_2(0)$, msec^{-1}	1.8	1.8	1.8
$\gamma = 3 \times 10^{-11}$ mho		A_{-2}, mV^{-1}	1×10^{-2}	1×10^{-2}	1×10^{-2}
$\gamma_{Na}/\gamma_K = 2.1$		$k_3(0)$, M^{-1} msec^{-1}	2.4×10^4	9.5×10^3	1.2×10^4
$V_{Na} = +50$ mV		A_3, mV^{-1}	-1×10^{-2}	-1.0×10^{-4}	-3.0×10^{-3}
$V_K = -100$ mV		$k_{-3}(0)$, msec^{-1}		1.0×10^{-3}	1.8
		A_{-3}, mV^{-1}		1.0×10^{-2}	1.0×10^{-2}
		$k_4(0)$, msec^{-1}	10.0		
		A_4, mV^{-1}	6×10^{-2}		

was found that a modified Euler method employed by Moore and Ramon (36) produced similar results [within 8% of the Runge-Kutta values for peak currents and 2.3% for half-decay times; time increment (Δt) = 10 μsec]. The major advantage of this technique was that the calculation time was reduced by about 50%. For most runs, Δt was set between 5 and 20 μsec. Above 20 μsec the numerical solution (with either method) failed to converge and the simulated EPC waveforms exhibited oscillations.

Two subroutines for analyzing the simulated EPCs could be called from the disc by the main program. The first was designed to calculate the peak current, time to peak, and half-decay time of EPCs with a single exponential decay phase. With user-computer interaction, the second program was able to separate the slopes of calculated EPCs with double exponential falling phases. After the user manually positioned four cursors along the semilogarithmic display of the biphasic EPC, the program calculated the magnitude of the slow terminal phase (extrapolated zero-time value), its slope, and the "peeled" slope of the initial phase. From the slope calculation, the respective half-decay times could then be determined.[3]

Sources of error. The nonuniformity in the smoothness of some of the theoretical log dose-response curves was due to computer round-off errors. Other sources of error included (a) the inaccuracy of manually positioning cursors with the LPS-11 potentiometers, an error manifest in the theoretical curves of Figs. 6, 7C, and 13, and (b) errors involved in exponential decomposition of scopolamine-altered EPCs, especially in estimating the half-time of the initial decay component (Figs. 7C and 13). Similar problems have also been reported elsewhere (18).

Determination of rate constants. Of the five rate constants describing the normal EPC, two (k_2 and k_{-2}) were assumed to be voltage-dependent, and the others voltage-independent (24, 37). The combined rate constant for acetylcholine removal (k_h) was fixed at 15 msec^{-1} for all simulations. The hydrolytic component (14.5 msec^{-1}) was obtained from velocity measurements on acetylcholinesterase under pseudo-first-order conditions (38). The diffusional component (0.5 msec^{-1}) was obtained from theoretical calculations of free diffusion from a geometric region resembling the amphibian neuromuscular junction (39).

In contrast to Magleby and Stevens (23, 24), we did not assume the rate constant for normal channel closing (k_{-2}) to be identical with the experimentally determined rate constant for the EPC decay. This difference arose because in the present study finite values were assigned to f, k_1, and k_{-1}. The control data in Fig. 10 were thus used to calculate the lower limits for $k_{-2}(0)$ and A_{-2}, which were later employed as initial values during the iterative computer runs (see below). The form of k_{-2} was still expressed by

$$k_{-2}(V) = k_{-2}(0)e^{A_{-2}V}$$

where $k_{-2}(0)$ is the decay rate constant in the absence of an electric field and A_{-2} describes the voltage sensitivity of channel closing. A relationship analogous to the above was used for k_2:

$$k_2(V) = k_2(0)e^{A_2V}$$

where $k_2(0)$ is the opening rate constant at 0 mV and A_2 describes the voltage sensitivity of channel opening.

Values for k_2, k_{-2}, k_1, and k_{-1} were obtained in conjunction with the previously described f, k_h, $[R]_{tot}$, and $[ACh]_{tot}$, using the following procedure. First, k_2 and k_{-2} were set to $0.693/\overline{HDT}$ ($\overline{HDT}$ = average control half-decay time at −90 mV), and k_1 and k_{-1} were allowed to vary; k_1 was scaled in order to permit both it and k_{-1} to be altered within the same numerical limits, i.e., between 1 and 50. Several combinations yielded theoretical EPCs that qualitatively resembled experimental currents. One of these sets was selected for the study. Next, the initial estimates of k_2 and k_{-2} were adjusted by computing EPCs over a wide range of membrane potentials and systematically varying $k_2(0)$, A_2, $k_{-2}(0)$, and A_{-2}. Combinations of these rate constants giving

[3] Copies of these programs are available from Dr. Albuquerque on request.

model waveforms whose amplitudes, rise, and half-decay times resembled experimental data (as judged by visual comparison) were considered acceptable. A limited number of combinations conformed to this criterion, from which the group appearing in Table 1 was selected for the study.

After the control rate constants were determined, k_3 and k_{-3} were chosen in model II. For scopolamine, the data shown in Fig. 13 were used to estimate lower limits for drug binding and dissociation reactions. Repetitive program runs were again utilized to find suitable values for these constants. The forward rate constant for atropine (k_3) was similarly obtained using the data in Fig. 10 as a lower limit. The value of k_{-3} for atropine, however, was always assumed to be near zero [$k_{-3}(0) = 1.0 \times 10^{-3}$ msec^{-1}]; A_{-3} was arbitrarily set at 1.0×10^{-2} mV^{-1}. Simulated EPCs were considered acceptable by the waveform criteria at various holding potentials used for control EPCs and by conformity to the experimentally obtained log dose-response relationships at −90 mV.

The rate constants in model I could not be directly approximated from the experimental results. Consequently these values were chosen solely on the basis of their ability to produce atropine- and scopolamine-like effects at different holding potentials and drug concentrations.

RESULTS

The rise and fall in the concentrations of ACh, ACh_2R, and ACh_2R^*, relative to the time course of the resulting model EPC, are shown in Fig. 1A. The temporal relationships are seen clearly in Fig. 1B, where the traces are displayed on an expanded time scale. The reactions are initiated by the arrival of acetylcholine, which is delivered to the model system for 300 μsec. This results in an early, rapid increase in acetylcholine concentration, followed by a much slower increase as transmitter molecules react to form ACh_2R, or leave the system via diffusional and hydrolytic routes. Once release is terminated, diffusional and hydrolytic losses bring about a rapid decline of acetylcholine concentration, such that only 7% of the initial acetylcholine remains

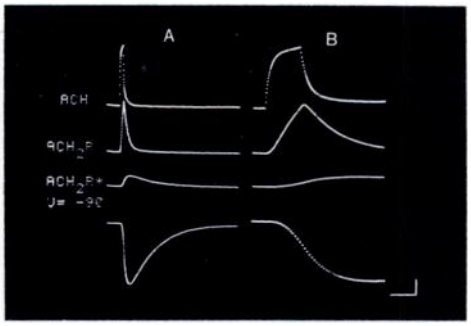

FIG. 1. *Concentration-time curves showing rise and fall of acetylcholine, ACh_2R, and ACh_2R^* concentrations and resulting EPC (at −90 mV) on a conventional (A) and expanded (B) time base*

Calibrations: vertical, 1×10^{-7} A or 0.18 μM; horizontal, 2 msec (A) and 0.2 msec (B).

by the time the EPC reaches its peak (0.60 msec). The conformational changes leading to the formation and decay of ACh_2R^* are much slower than the rates of transmitter release, binding, dissociation, and removal, and show an exponential dependence on membrane potential. Because these conformational changes are slow relative to the voltage-independent reactions, only a small fraction of ACh_2R is converted to the activated ACh_2R^*. From assumption (a), the concentration of ACh_2R^* is proportional to the concentration of open channels, and therefore the concentration-time curve of ACh_2R^* determines the time course of the EPC. It should be noted, however, that the above description reflects the assumptions made earlier, and therefore a consistent picture cannot be taken as evidence for the validity of the underlying process.

Figure 2 shows families of simulated (Fig. 2A) and experimentally obtained (Fig. 2B) EPCs at potentials between +20 and −140 mV. Variations in membrane potential reveal the existence of two voltage-dependent processes associated with the normal EPC. First, the relationship between EPC amplitude and membrane potential is not strictly linear, but exhibits an upward curvature in the hyperpolarized region (23, 24, 40). It has been proposed (31) that the curvature in the (end plate) current-voltage relationship results from a decrease in the rate constant for channel opening (k_2) with large negative

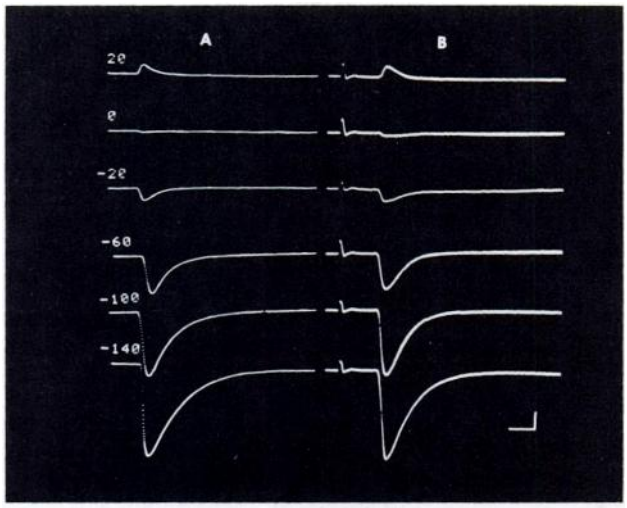

FIG. 2. *Families of EPCs from model III (A) compared with records from a frog sartorius muscle fiber (B)* The experimental traces were obtained by displacing the membrane potential in 10-mV steps from the holding potential of −100 mV. Calibrations: vertical, 1×10^{-7} A; horizontal, 2 msec.

potentials. Thus, with increasing hyperpolarization, progressively fewer channels would be open during the EPC peak, giving rise to the observed nonlinearity.

Second, the half-decay time of the normal EPC varies (exponentially) with membrane potential (23, 40). In the records of Fig. 2B, the half-decay time exhibited a 2-fold lengthening for a 100-mV hyperpolarization. The effect of voltage on the EPC decay was suggested by Magleby and Stevens (24) to result from the influence of the membrane electric field on the rate constant for channel closing (k_{-2}).

The simulated family of EPCs (Fig. 2A) was obtained by assuming that the curvature in the current-voltage relationship and the lengthening in the half-time of decay were manifestations of the voltage sensitivities of k_2 and k_{-2}, respectively. These assumptions resulted in model waveforms whose amplitudes, rise times and half-decay times corresponded closely with the experimental records.

Sequential Models for Drug Action

The essential differences between sequential models I and II are illustrated in Fig. 3. Simulations of drug-altered EPCs by model II are shown in Fig. 3A for 150 μM atropine and in Fig. 3B for 25 and 150 μM scopolamine. The drug-free condition is denoted by the uppermost ACh_2R^* curve, the lowermost EPC trace, and the absence of the ACh_2R^*D complex. When a drug such as atropine or scopolamine is present, a fraction of the active ACh_2R^* is converted to the inactive ACh_2R^*D complex. The effect of this conversion will be a more rapid initial decay of ACh_2R^* and a decrease in its peak amplitude.

The factor that determines whether ACh_2R^* will continue to decay at its rapid initial rate is k_{-3}. By making k_{-3} suitably small ($\leqq 0.004$ msec^{-1} at −90 mV), the ACh_2R^*D complex becomes sufficiently stable so that no appreciable accumulation of ACh_2R^* occurs from removal of D. The resulting EPC will then show the rapid, simple exponential decay characteristic of the atropine effect. As k_{-3} is raised, the more rapid dissociation of ACh_2R^*D will cause ACh_2R^* to persist for several milliseconds. Consequently the rapid initial decay of ACh_2R^* is superseded by a slow terminal component. These alterations are reflected in the EPC, which exhibits the biphasic decay characteristic of the scopolamine response.

Figure 3C illustrates the production of abbreviated EPC decays by model I. To simulate such waveforms, Steinbach (5) assumed that ACh_2R^*D is inactive; hence, in this case, the two models differ only in the ultimate fate of ACh_2R^*D. But since no

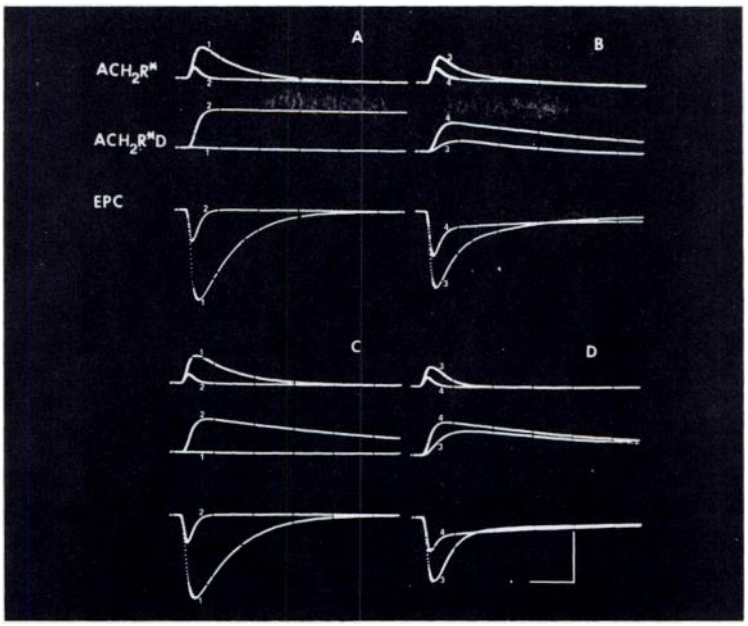

FIG. 3. *Superimposed concentration-time curves for ACh_2R^*, ACh_2R^*D, and resulting EPC (at −90 mV) to illustrate basic differences between the two sequential models*

Model II is represented by the records in A and B. Figure $3A_1$ indicates control conditions; A_2 shows the effects of 150 μM atropine. Figure $3B_3$ and B_4 show, respectively, the effects of 25 and 150 μM scopolamine. Model I is represented by the records in C and D. Figure $3C_1$ indicates control conditions; C_2 shows the effects of 150 μM atropine. Figure $3D_3$ and D_4 show, respectively, the effects of 25 and 150 μM scopolamine. Note that model II predicts a decrease in the decay rate of the terminal component with an increase in scopolamine concentration, while model I predicts that the terminal decay rate will be independent of drug concentration. Calibrations: vertical, 2×10^{-7} A or 0.22 μM; horizontal, 4 msec.

measurable current accompanies either the dissociation of ACh_2R^*D to free reactants, as postulated by model I, or the very slow elimination of D from ACh_2R^*D, as suggested for model II, either model is capable of simulating atropine-altered EPCs.

The models differ considerably, however, in their simulation of biphasic EPC decays. Unlike model II, the terminal component in model I is produced by residual conductance of the ACh_2R^*D complex. The relevant traces for model I are shown in Fig. 3D for 25 and 150 μM scopolamine. Addition of drug results in the rapid conversion of ACh_2R^* to the less active ACh_2R^*D ($\gamma_{ACh_2R^*D} = 0.125\ \gamma ACh_2R^*$), which then decays slowly as it dissociates to free reactants. Raising the drug concentration causes an increase in the rate of conversion of ACh_2R^* to ACh_2R^*D and a greater accumulation of ACh_2R^*D, but no change in its decay rate. Thus model I predicts that in the presence of scopolamine, the magnitude of the terminal current should increase with increases in drug concentration, while its decay rate should be independent of concentration. These predictions are in conflict with the data. In contrast, model II predicts the experimentally observed reduction in the magnitude of the terminal current, and slowing of its decay rate with increases in drug concentration. These and other predictions of the kinetic models are tested in Figs. 4–13.

Simulations of Atropine-Altered EPCs

Figure 4A (right) shows EPCs at −90 mV from a muscle fiber exposed to atropine concentrations ranging from 60 to 600 μM. Increases in atropine concentration result in depression of the peak EPC amplitude and shortening in the rise and half-decay times. The decay phase remains a predominantly simple exponential function of time at all concentrations. These effects are accurately simulated by sequential model II,

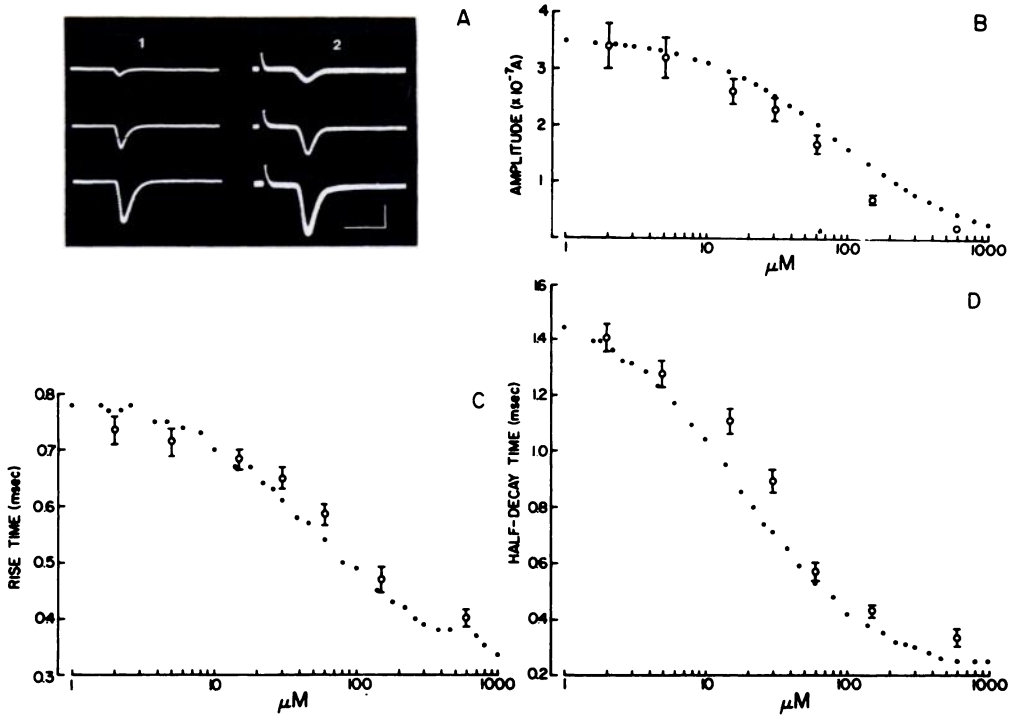

FIG. 4. *Dose-response relationships demonstrating that sequential model II can simulate actions of atropine on EPC*

A. Waveforms predicted by model II (1) are compared with records from a muscle fiber (2) following exposure to 60 μM (bottom), 150 μM (center), and 600 μM (top) atropine. Calibrations: vertical, 1×10^{-7} A; horizontal, 2 msec. Figure 4B, C, and D are dose-response relationships for depression of peak EPC amplitude, reduction of the rise time, and shortening of the half-decay time in the presence of the indicated concentrations of atropine. ○ and vertical bars, means ± standard errors of data pooled from 12–21 muscle fibers; ●, predictions from sequential model II. Some of the experimental values are based on a larger sample size and therefore differ slightly from those reported before (13). The holding potential was −90 mV.

as indicated by the traces on the left. To obtain such waveforms, the parameter *D* in model II was adjusted to produce the indicated drug concentrations with an assumed synaptic cleft volume of 10^{-11} liter. Changes in *D* were found to be sufficient to explain the full extent of the action of atropine over the 10-fold concentration range illustrated.

Using the rate constants and parameters that produced the waveforms of Fig. 4A, sequential model II was able to simulate the concentration-effect relationships for depression of the peak EPC amplitude, reduction in the time to peak, and shortening in the half-decay time, as shown in Fig. 4B–D. The open circles and vertical bars represent the means ± standard errors of EPC amplitudes and rise and half-decay times obtained from 12–21 end plates at various concentrations of atropine. The filled circles are the corresponding values simulated from model II. The model correctly predicts the experimentally observed concentration-effect relationships, as shown by the close agreement between the data points and the simulated values. Although the preceding simulations were derived from model II, the effects of atropine could also be described adequately by model I. This was not the case for scopolamine, for which model II was clearly superior.

Simulations of Scopolamine-Altered EPCs

Several alterations of the EPC accompany increases in scopolamine concentrations at a fixed membrane potential. These include (a) shortening in the time to peak,

(b) acceleration of the initial decay rate, (c) slowing of the terminal decay rate, (d) reduction of the peak amplitude, and (e) suppression of both the absolute and relative magnitudes of the terminal current.

In model I, biphasic decays were produced by setting ACh_2R^*D/ACh_2R^* conductances equal to 0.125 and adjusting k_3 and k_4 to fit the initial and terminal components, respectively, of EPCs recorded in the presence of 150 μM scopolamine. When D was changed to higher or lower concentrations, the half-decay time of the terminal component was found to be concentration-independent, while its magnitude increased with increases in concentration (Fig. 5). The greatest discrepancy between model I and data occurred with 600 μM scopolamine, for which the extrapolated zero-time value of the terminal component comprised less than 10% of the experimental EPC, but almost all of the EPC generated from model I. To obtain better agreement with the data, it would be necessary to make the arbitrary assumption that the relative conductance of ACh_2R^*D varies with drug concentration, as well as the improbable assumption that the rate constant k_4 changes with concentration. For sequential model II, however, changes in D sufficed to produce the correct variation in the magnitude and decay rate of the terminal component.

In Fig. 6 the ratio of the terminal to peak currents is plotted as a function of scopolamine concentration. If the simulations are extended to a wider concentration range, model II is seen to approximate the experimentally observed variation in the relative magnitude of the terminal component. The predictions from model I, by contrast, deviate from the experimental values, except for the single point occurring at the intersection of the two curves.

Figure 7 shows that model II can also account quantitatively for the effect of scopolamine on the EPC amplitude, rise time, and half-times of the initial and terminal decay components. Thus, at a fixed membrane potential, the effects of scopolamine on the EPC appear to be well described by

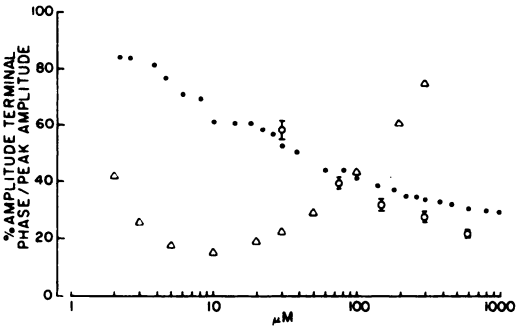

FIG. 6. *Dose-response relationships at −90 mV for scopolamine-induced depression in relative magnitude of terminal decay component*

○ and vertical bars, means ± standard errors of data pooled from 6–22 fibers; △ and ●, predictions from models I and II, respectively.

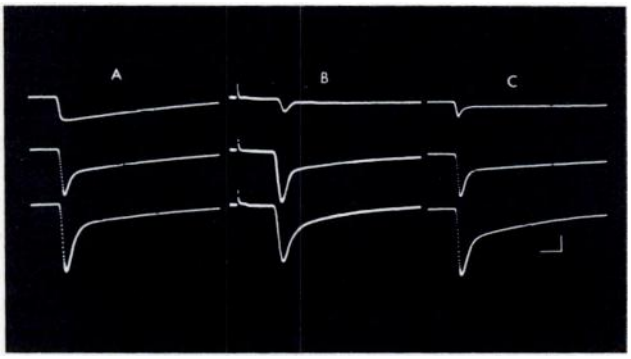

FIG. 5. *EPCs simulated from sequential models I (A) and II (C) compared with experimental records (B) at three concentrations of scopolamine*

Bottom, 60 μM; center, 150 μM; top, 600 μM scopolamine. The depression in the relative magnitude of the terminal decay component and lengthening in its half-decay time with increases in scopolamine concentration are accurately predicted by model II but not by model I. Calibrations: vertical, 1×10^{-7} A; horizontal, 2 msec. The holding potential was −90 mV.

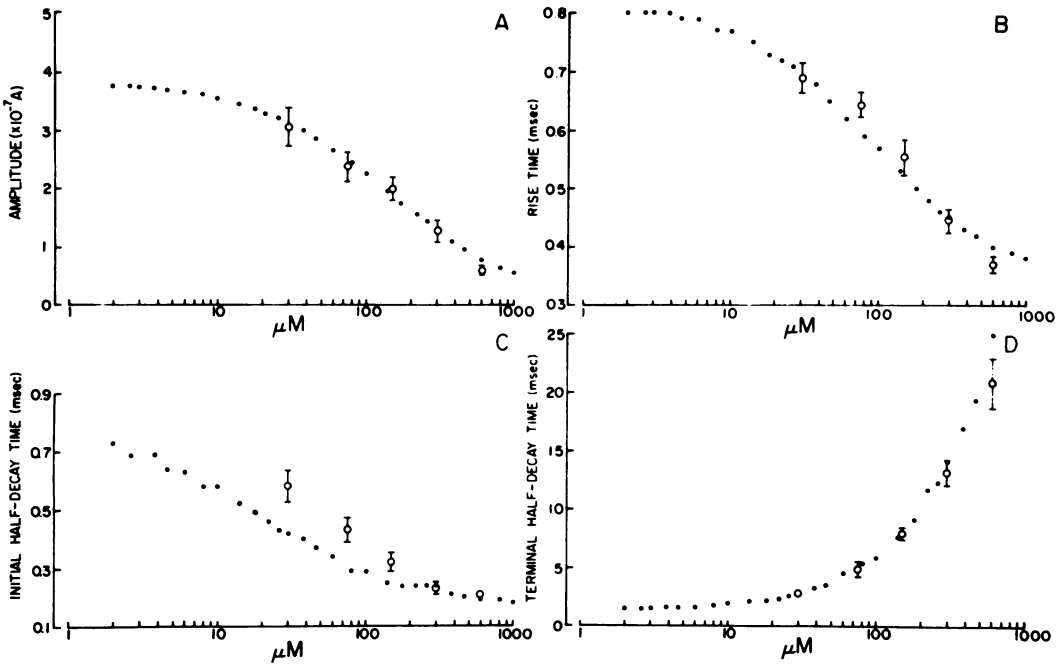

FIG. 7. *Dose-response relationships for actions of scopolamine on peak amplitude (A), rise time (B), and half-decay times of initial (C) and terminal (D) decay components*

○ and vertical bars, means ± standard errors of experimental data pooled from 6–22 muscle fibers; ●, represent predictions from model II. Some of the experimental values are based on a larger sample size and therefore differ slightly from those reported before (13). The holding potential was −90 mV.

reversible binding of drug to the activated acetylcholine receptor and subsequent formation of an inactive complex. The model, which postulates irreversible drug binding, a partially active ACh_2R^*D, and its dissociation to free reactants, is in conflict with the experimental data.

Predictions of Models at Other Membrane Potentials

EPCs recorded between −140 and +20 mV in the presence of atropine (60 μM) are shown in Fig. 8. Variations in the membrane potential reveal two additional actions of atropine: (a) the nonlinearity in the relationship between peak amplitude and membrane potential is enhanced, and (b) the half-decay time becomes less dependent on membrane potential. Both observations suggest that the action of atropine is voltage-dependent. This feature was incorporated in the kinetic models by making k_3, k_{-3}, and k_4 exponential functions of membrane potential of the form $k_j = k_j(0)e^{A_jV}$. In model II the voltage-sensitive term (A_j)

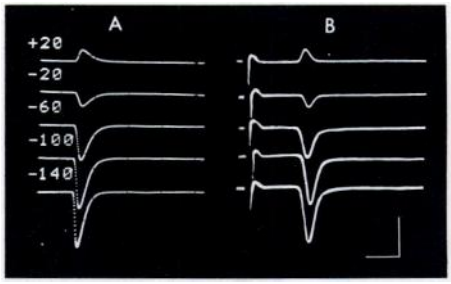

FIG. 8. *Families of EPCs in the presence of 60 μM atropine*

The records on the left (A) were obtained from sequential model II. The traces on the right (B) were recorded from a single muscle fiber by shifting the membrane potential in 10-mV steps from the holding potential of −100 mV. Calibrations: vertical, 1×10^{-7} A; horizontal, 2 msec.

was negative for k_3, causing drug binding to increase with hyperpolarization. A positive A_{-3} was required in order to make the dissociation of ACh_2R^*D slower with hyperpolarization. Using the previously derived values for $k_3(0)$, A_3; $k_{-3}(0)$, A_{-3}; and $k_4(0)$, A_4, both sequential models were able to

simulate the curvature in the current-voltage relationship and the departure of the half-decay time from membrane potential. The relevant plots from model II are shown in Fig. 9 for the effect of atropine (60 μM) on the current-voltage relationship and in Fig. 10 for its effect on the relationship between half-decay time and membrane potential. As indicated in these figures, model II, with the same pair of voltage-sensitive rate constants, was able to describe simultaneously the increase in the curvature of the current-voltage relationship and the decrease in the voltage dependence of the decay phase.

The corresponding data for scopolamine are presented in Figs. 11–13. In the presence of scopolamine (150 μM), hyperpolarization causes the terminal component to decay more slowly, and its relative magnitude to become suppressed. These alterations resemble increases in scopolamine concentration at a fixed membrane potential (Fig. 5). The waveforms generated by model II dis-

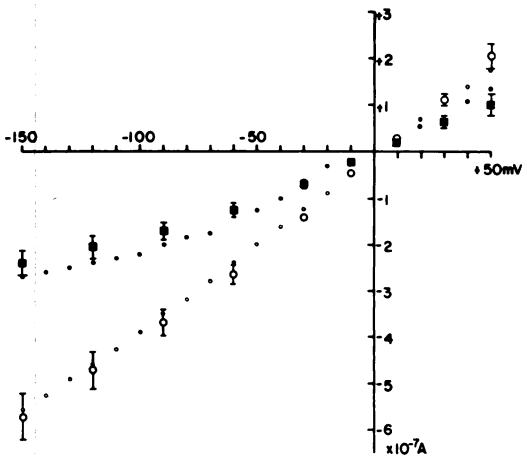

FIG. 9. *Current-voltage plots illustrating relationship between peak EPC amplitude and membrane potential in control* (○) *and in the presence of 60 μM atropine* (■)

Each symbol represents the mean ± standard error of 12–22 fibers. The small open and filled circles are predictions from sequential model II for control and 60 μM atropine, respectively.

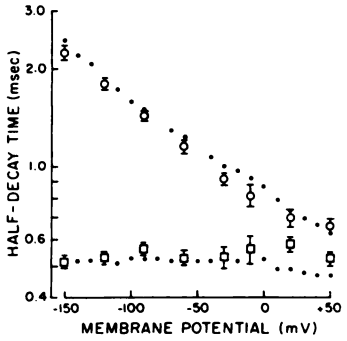

FIG. 10. *Semilogarithmic plots illustrating relationship between EPC half-decay time and membrane potential in control* (○) *and in the presence of 60 μM atropine* (□)

Each symbol represents the mean ± standard error of 12–18 fibers. The small filled circles are predictions from sequential model II.

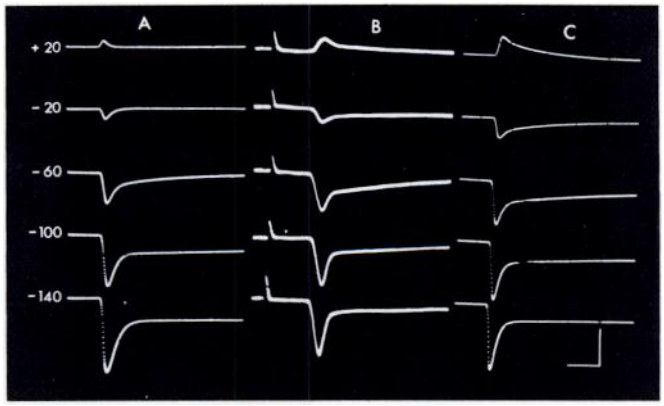

FIG. 11. *Families of EPCs in the presence of scopolamine (150 μM)*

The predictions from sequential models I (A) and II (C) are compared with experimentally obtained EPCs (B). Note that model I predicts an increase in the relative magnitude of the terminal decay component with hyperpolarization, while model II and data show the opposite change. Calibrations: vertical, 1×10^{-7} A; horizontal, 2 msec.

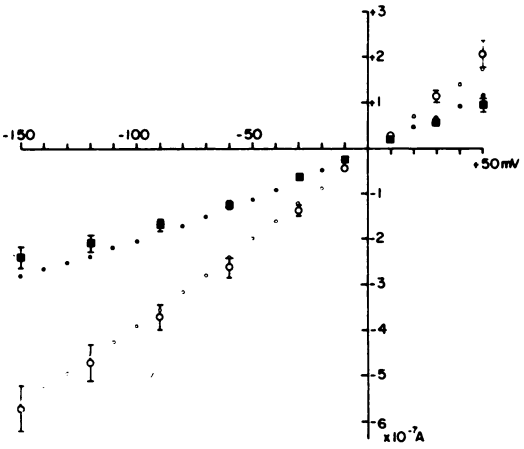

FIG. 12. *Current-voltage plots illustrating relationship between peak EPC amplitude and membrane potential in control* (○) *and in the presence of 150 μM scopolamine* (■)

Each symbol represents the mean ± standard error of 13–22 fibers. The small open and filled circles are predictions from sequential model II for control and 150 μM scopolamine, respectively.

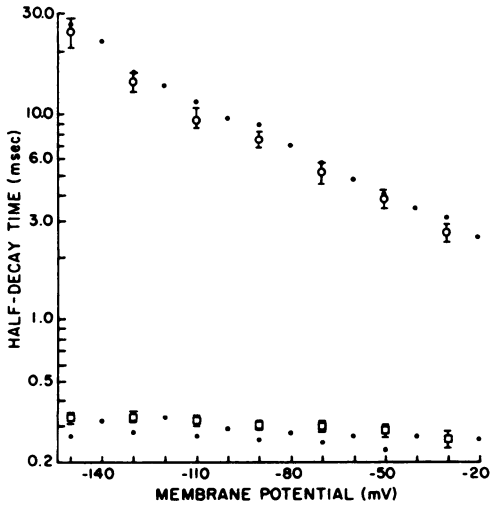

FIG. 13. *Semilogarithmic plots illustrating relationship between half-decay time of initial* (□) *and terminal* (○) *decay components of EPC in the presence of 150 μM scopolamine*

Each symbol represents the mean ± standard error of 6–10 fibers. The small filled circles are predictions from sequential model II.

played both experimental alterations (Fig. 11C), in agreement with the data (Figs. 12 and 13). For model I, however, even when k_3 and k_4 were adjusted to conform to the experimentally observed initial and terminal decay rates, it was not possible to obtain simultaneous agreement with voltage-dependent changes in the relative magnitude of the terminal current (Fig. 11A).

DISCUSSION

The results of this investigation indicate that sequential model II can account for the effects of atropine and scopolamine on the EPC. The basic feature of the sequential class of models is the drug-mediated conversion of the end plate channel from a transient state of high conductance to a prolonged state of low or zero conductance. Although both models can simulate the abbreviated EPC decays observed in atropine, only sequential model II was able to simulate the biphasic EPC decays occurring in the presence of scopolamine. The shortcomings of model I, as revealed by this study, were the assumptions that the formation and dissociation of ACh_2R^*D was irreversible and that ACh_2R^*D was partially conducting. Models based on these assumptions will generate terminal components whose magnitudes increase with increases in drug concentration, and whose decay rates are independent of concentration. From inspection of reaction scheme I and Fig. 3D, it is clear that the discrepancies between model I and the data do not result from the particular rate constants used, but rather from the assumption that the terminal decay component represents the slow dissociation of a partially active ACh_2R^*D complex.

These assumptions were abandoned in formulating sequential model II. In this model, ACh_2R^*D was considered to be inactive under all conditions, so that only one conducting species (ACh_2R^*) occurs in both the absence and presence of drug. Furthermore, the ACh_2R^*D complex was assumed to dissociate by elimination of drug to reconstitute ACh_2R^*, instead of by dissociation to free reactants. With these assumptions, the model was able to simulate the alterations in the magnitude and decay rate of the terminal component with changes in drug concentration (Figs. 6 and 7D) and membrane potential (Figs. 11 and 13). The assumption of zero conductance for ACh_2R^*D was not made arbitrarily, but

was necessary to obtain optimal agreement with the experimentally observed magnitude of the terminal component (Fig. 6). Any residual conductance of ACh_2R^*D, regardless of how small, tended to produce deviation from experimental values.

At present, reaction scheme II appears to be the most satisfactory kinetic model for describing the actions of atropine and scopolamine on the EPC. Its predictions are consistent not only with our results (11–13, 25) but with those of other investigators as well (9, 14, 41). Similar models have also been proposed for EPCs altered by local anesthetics (42) and have produced satisfactory agreement with experimental data (43, 44).

In addition, model II can account for the shortening in the EPC rise and half-decay times and the reduction in the voltage sensitivity of the EPC decay in the presence of histrionicotoxin and its structural analogues (16). However, model II, using the rate constants in Table 1, does not predict the hysteresis in the current-voltage relationship or the progressive depression of peak amplitude with repetitive nerve stimulation observed in the presence of histrionicotoxin. Markedly different rate constants or additional drug sites are required to reproduce these observations.

Modifications of the sequential model to include additional drug sites have been proposed for procaine, atropine, and histrionicotoxin (16, 45, 46). Recently Adams (45), using voltage jump-relaxation techniques, reported that his cyclic model was the simplest one capable of explaining both kinetic and equilibrium observations with procaine. The cyclic model requires binding of drug to R as well as to ACh_nR^*, and interconversion of the resulting RD and ACh_nR^*D complexes. The model proposed by Feltz *et al.* (46) also postulates drug binding to both open and closed channels but does not require interconversion of the drug-channel complexes. In this case, the closed channel binding was invoked to account for the depression of peak EPC amplitude observed in the presence of atropine. In our study, the reduction of EPC amplitude could be explained satisfactorily without assuming that atropine reacts with either R or ACh_nR (Fig. 4B). Although our finding does not exclude an affinity of atropine for the closed channel, the close correspondence between the data and predictions based solely on binding to the open channel indicates that other sites contribute little to the depression of EPC amplitude.

It has recently been reported that under conditions of low drug concentration and depolarized membrane potentials, EPCs in the presence of the lidocaine derivative QX-222 decayed as the sum of three exponentials (18, 44). In addition to the fast and slow decay components described for scopolamine, QX-222-altered EPCs showed an intermediate component having voltage sensitivities and decay rates similar to those of control EPCs. The intermediate component, according to Beam (18), represents a population of unaltered channels, which is converted to rapidly and slowly decaying forms with hyperpolarization and increases in drug concentration. This proposal requires local anesthetic molecules to act before receptor activation, and is compatible with the sequential model if the initial binding of drug with R leads to a modified form capable of being blocked in the open conformation (44).

An intermediate decay component with normal characteristics was not observed with scopolamine-altered EPCs in the present study; most EPCs were fitted accurately by two exponentials. Additional components were encountered occasionally, but these did not decay at control rates and did not show a consistent dependence on drug concentration or membrane potential (see Figs. 4 and 8 of ref. 13). This discrepancy may be related to differences between QX-222 and scopolamine or to the different methods of exponential decompositions.

The most attractive feature of model II is that it describes all effects of atropine and scopolamine on the EPC by a single mechanism, which is that the drugs bind to the activated transmitter-receptor complex in a voltage-dependent manner to produce an inactive complex. If elimination of drug from this complex is slow relative to the normal closing rate of channels, the resulting EPC will show the abbreviated simple exponential decay characteristic of the atropine response. More rapid elimination

will lead to secondary accumulation of ACh_2R^*, and hence to the terminal component characteristic of the scopolamine response. Thus, although the EPCs appear different in the presence of the two drugs, their underlying mechanisms may be similar; if model II is essentially correct, atropine and scopolamine differ only in the stability of the hypothetical ACh_2R^*D complex. According to the model, the shortening in the rise time and depression of peak amplitude occur secondarily from the more rapid decay. This mechanism alone is sufficient to account for the experimentally observed changes in amplitude and rise time in the presence of both atropine (Fig. 4B and C) and scopolamine (Fig. 7A and B). The depression in EPC amplitude arises from the fact that the drug-altered channel spends an appreciable fraction of its lifetime in the blocked state, and the current passing through these channels is therefore diminished. The curvature in the current-voltage relationship (Figs. 9 and 12) and the alteration in the relationship between half-decay time and membrane potential (Figs. 10 and 13) follow directly from the assumption that drug binding and retention increase with membrane hyperpolarization.

ACKNOWLEDGMENTS

The authors thank Ms. Mabel Alice Zelle for technical assistance, and Mrs. Margaret Shimkaveg for help in preparation of the manuscript.

REFERENCES

1. Furukawa, T. (1957) *Jap. J. Physiol.*, **7**, 199–212.
2. Maeno, T. (1966) *J. Physiol. (Lond.)*, **183**, 592–606.
3. Gage, P. W. & Armstrong, C. M. (1968) *Nature*, **218**, 363–365.
4. Steinbach, A. B. (1968) *J. Gen. Physiol.*, **52**, 144–161.
5. Steinbach, A. B. (1968) *J. Gen. Physiol.*, **52**, 162–180.
6. Kordaš, M. (1970) *J. Physiol. (Lond.)*, **209**, 689–699.
7. Beránek, R. & Vyskočil, F. (1967) *J. Physiol. (Lond.)*, **188**, 53–66.
8. Beránek, R. & Vyskočil, F. (1968) *J. Physiol. (Lond.)*, **195**, 493–503.
9. Kordaš, M. (1968) *Int. J. Neuropharmacol.*, **7**, 523–530.
10. Magazanik, L. G. & Vyskočil, F. (1969) *Experientia*, **25**, 618–619.
11. Adler, M. & Albuquerque, E. X. (1974) *Pharmacologist*, **16**, 233.
12. Adler, M. & Albuquerque, E. X. (1974) *Abstr. 4th Annu. Meet. Soc. Neurosci. (St. Louis)*, p. 113.
13. Adler, M. & Albuquerque, E. X. (1976) *J. Pharmacol. Exp. Ther.*, **196**, 360–372.
14. Feltz, A. & Large, W. A. (1976) *Br. J. Pharmacol.*, **56**, 111–113.
15. Albuquerque, E. X., Barnard, E. A., Chiu, T. H., Lapa, A. J., Dolly, J. O., Jansson, S.-E., Daly, J. & Witkop, B. (1973) *Proc. Natl. Acad. Sci. U. S. A.*, **70**, 949–953.
16. Albuquerque, E. X., Kuba, K. & Daly, J. (1974) *J. Pharmacol. Exp. Ther.*, **189**, 513–524.
17. Eldefrawi, A. T., Eldefrawi, M. E., Albuquerque, E. X., Oliveira, A. C., Mansour, N., Adler, M., Daly, J. W., Brown, G. B., Burgermeister, W. & Witkop, B. (1977) *Proc. Natl. Acad. Sci. U. S. A.*, **74**, 2172–2176.
18. Beam, K. G. (1976) *J. Physiol. (Lond.)*, **258**, 279–300.
19. Beam, K. G. (1976) *J. Physiol. (Lond.)*, **258**, 301–322.
20. Maeno, T., Edwards, C. & Hashimura, S. (1971) *J. Neurophysiol.*, **183**, 592–606.
21. Deguchi, T. & Narahashi, T. (1971) *J. Pharmacol. Exp. Ther.*, **176**, 423–433.
22. del Castillo, J. & Katz, B. (1957) *Proc. R. Soc. Lond., Ser. B, Biol. Sci.*, **146**, 369–381.
23. Magleby, K. L. & Stevens, C. F. (1972) *J. Physiol. (Lond.)*, **223**, 151–171.
24. Magleby, K. L. & Stevens, C. F. (1972) *J. Physiol. (Lond.)*, **223**, 173–197.
25. Adler, M., Albuquerque, E. X. & Lebeda, F. J. (1976) *Neurosci. Abstr.*, **2**, 699.
26. Gage, P. W. & Eisenberg, R. S. (1969) *J. Gen. Physiol.*, **53**, 279–297.
27. Takeuchi, A. & Takeuchi, N. (1959) *J. Neurophysiol.*, **22**, 395–411.
28. Kuba, K., Albuquerque, E. X., Daly, J. & Barnard, E. A. (1974) *J. Pharmacol. Exp. Ther.*, **189**, 499–512.
29. Box, G. E. P., Cousins, W. R., Davies, O. L., Hinsworth, F. R., Kenney, H., Milbourn, M., Spendley, W. & Stevens, W. L. (1967) in *Statistical Methods in Research and Production with Special Reference to the Chemical Industry* (Davies, O. L., ed.), Oliver and Boyd, London.
30. Albuquerque, E. X., Barnard, E. A., Porter, C. W. & Warnick, J. E. (1974) *Proc. Natl. Acad. Sci. U. S. A.*, **71**, 2818–2822.
31. Dionne, V. E. & Stevens, C. F. (1975) *J. Physiol. (Lond.)*, **251**, 245–270.
32. Barnard, E. A., Wieckowski, J. & Chiu, T. H. (1971) *Nature*, **243**, 207–209.
33. Barnard, E. A., Dolly, J. O., Porter, C. W. & Albuquerque, E. X. (1975) *Exp. Neurol.*, **48**, 1–28.

34. Hubbard, J. I., Llinás, R. & Quastel, D. M. J. (1969) *Electrophysiological Analysis of Synaptic Transmission,* Williams & Wilkins, Baltimore.
35. Weeg, G. P. & Reed, G. B. (1966) *Introduction to Numerical Analysis,* Blaisdell, London.
36. Moore, J. W. & Ramon, F. (1974) *J. Theor. Biol.,* **45,** 249–273.
37. Anderson, C. R. & Stevens, C. F. (1973) *J. Physiol. (Lond.),* **235,** 655–691.
38. Froede, H. C. & Wilson, I. B. (1971) in *The Enzymes* (Boyer, P. D., ed.), Vol. 5, pp. 87–114, Academic Press, New York.
39. Eccles, J. C. & Jaeger, J. C. (1958) *Proc. R. Soc. Lond., Ser. B, Biol. Sci.,* **148,** 38–56.
40. Kordaš, M. (1969) *J. Physiol. (Lond.),* **204,** 493–502.
41. Katz, B. & Miledi, R. (1973) *Proc. R. Soc. Lond., Ser. B, Biol. Sci.,* **184,** 221–226.
42. Adams, P. R. (1975) *J. Physiol. (Lond.),* **246,** 61P–63P.
43. Katz, B. & Miledi, R. (1975) *J. Physiol. (Lond.),* **249,** 269–284.
44. Ruff, R. L. (1977) *J. Physiol. (Lond.),* **264,** 89–124.
45. Adams, P. R. (1977) *J. Physiol. (Lond.),* **268,** 291–318.
46. Feltz, A., Large, W. A. & Trautmann, A. (1977) *J. Physiol. (Lond.),* **269,** 109–130.